



LAWRENCE
LIVERMORE
NATIONAL
LABORATORY

LLNL-TR-767905

3D Moment Tensor Inversion of Underground Chemical Explosions from the Source Physics Experiments

A. Chiang, A. Pitarka, S. R. Ford, S. Ezzedine, O. Y. Vorobiev

February 14, 2019

Disclaimer

This document was prepared as an account of work sponsored by an agency of the United States government. Neither the United States government nor Lawrence Livermore National Security, LLC, nor any of their employees makes any warranty, expressed or implied, or assumes any legal liability or responsibility for the accuracy, completeness, or usefulness of any information, apparatus, product, or process disclosed, or represents that its use would not infringe privately owned rights. Reference herein to any specific commercial product, process, or service by trade name, trademark, manufacturer, or otherwise does not necessarily constitute or imply its endorsement, recommendation, or favoring by the United States government or Lawrence Livermore National Security, LLC. The views and opinions of authors expressed herein do not necessarily state or reflect those of the United States government or Lawrence Livermore National Security, LLC, and shall not be used for advertising or product endorsement purposes.

This work performed under the auspices of the U.S. Department of Energy by Lawrence Livermore National Laboratory under Contract DE-AC52-07NA27344.

1 **3D Moment Tensor Inversion of Underground Chemical Explosions from the 2 Source Physics Experiments**

3 **Andrea Chiang, Arben Pitarka, Sean R. Ford, Souheil Ezzedine and Oleg Y. Vorobiev**

5 **Abstract**

6 Several physical mechanisms have been proposed to explain the generation of S-waves
7 from underground explosions, such as asymmetries in the source, release of tectonic pre-stress,
8 interactions with the free-surface, spall, and heterogeneities in the Earth. An accurate description
9 of the explosion source processes is an important step towards understanding which of these
10 plausible mechanisms are actively contributing to the generation of S-waves and under what
11 conditions. In this study we explore the application of the seismic moment tensor source to model
12 far-field, low frequency (up to 6 Hz) waveform data of over-buried chemical explosions from the
13 Source Physics Experiment, with a focus on S-wave generation and amplitude predictions. We use
14 an inverse waveform modeling approach to estimate the source properties of the chemical
15 explosions, and compare solutions using different velocity models. 1D and 3D subsurface velocity
16 models are used to characterize wave propagation between the source and receiver. We also
17 performed analysis on wavefield simulations from physic-based explosion source modeling. The
18 analyses show scattering and phase conversion from 3D heterogeneities dominate the generation of
19 far-field, S-wave energy observed in data, and that the variability in the recovered deviatoric
20 component of the moment tensor source model are largely a result of inadequately accounting for
21 3D wave propagation effects in the inversion process.

23 **Introduction**

24 The development and validation of physics-based explosion source models is necessary to
25 improve our ability to predict seismic amplitudes from explosions. One key component to
26 predicting explosion amplitudes is the knowledge of mechanisms that are actively contributing to
27 the generation of S-waves and under what conditions. Several physical mechanisms have been
28 proposed to explain the generation of S-waves from underground explosions, such as asymmetries
29 in the source, release of tectonic pre-stress, interactions with the free-surface, spall, and
30 heterogeneities in the Earth (e.g. Wallace et al., 1985; Johnson and Sammis, 2001; Patton et al.
31 2005; Vorobiev et al. 2015). To address these questions the Source Physics Experiment (SPE) was
32 conducted in a hard rock geologic formation close to past underground nuclear tests. The
33 experiment is a long-term NNSA research and development effort to improve U.S. nuclear
34 nonproliferation verification and monitoring capabilities, including detection, identification and
35 yield determination of small nuclear tests. The 1993 Non-Proliferation Experiment (NPE) showed
36 that chemical explosions can be used as a proxy for seismic signals from nuclear explosions
37 because they produce similar seismic observables except with an overall amplitude scaling factor
38 (Denny et al., 1994). The goals of SPE are to advance current understanding of source
39 phenomenology, near-field wave propagation, coupling of energy into the seismic wavefield and
40 the generation of shear waves (Snelson et al., 2013). A comprehensive study of explosion-related
41 physical processes is crucial to replacing semi-empirical models with physics-based numerical
42 techniques.

43 In this study we explore the application of the moment tensor (MT) source to model far-
44 field (at distances within a few kilometers) seismic data from over-buried chemical explosions,
45 particularly on S-wave amplitude predictions, what are the recovered source properties (e.g.
46 moment, off-diagonal components of the tensor) and how they relate to depth of burial and

47 subsurface velocity structure. All of these questions are relevant to MT-based methods for event
48 discrimination and identification.

49

50 **Research Accomplished**

51 Waveform inversion to determine the seismic MT is a well-established method for
52 determining the source properties of natural and anthropogenic seismicity, and can identify, or
53 discriminate different types of seismic sources. The technique has been applied to underground
54 explosions and other anthropogenic events, as well as earthquakes from geothermal (Guilhem et
55 al., 2014) and volcanic environments (Shuler et al., 2013) and events induced by oil and gas
56 operations (McNamara et al., 2015). MT analysis were done on SPE velocity data recorded along
57 the five linear geophone arrays centered around the shot point. A few additional high-gain sensors
58 were included in 1D MT inversions but not 3D because these stations are located outside the 3D
59 Earth model domain.

60

61 *3D Moment Tensor Inversion*

62 Based on the representation theorem (Aki and Richards, 2002), velocities or displacements
63 in the n direction (e.g. transverse, radial and vertical) is expressed as a linear convolution of the
64 seismic MT and the spatial derivatives of the elastic Green's functions, assuming a point source
65 approximation:

$$66 \quad u_n(t, \vec{x}) = M_{ij} * G_{ni,j}(\vec{x}, t)$$

67 i and j are the directions of the forces and derivatives (force couples).

68 The seismic MT is a 3 by 3 symmetric tensor where the nine generalized force couples can
69 describe seismic sources including earthquakes, explosions, collapse, and volcanic eruptions. G is
70 the impulse response of the medium at the receiver along the direction x, y and z. We use WPP
71 (Wave Propagation Program) to calculate the Green's functions used in the 3D MT inversion. WPP
72 is an elastic finite-difference code for seismic waveform modeling (Xu et al., 2014). WPP solves
73 for the wave equation in Cartesian displacement formulation using a second order accurate
74 numerical method (Nilsson et al., 2007). The code handles purely elastic calculations but also
75 includes attenuation, topography, and arbitrary number of point force and/or moment tensor
76 source. WPP was also used in subsequent physic-based far-field waveform simulations.

77 Because of the linear relation between the six elements of the symmetric MT and
78 waveforms (u_n) the solution can be obtained using a least-squares formulation that minimizes the
79 misfit between observation and synthetics. Mathematically the inversion can be done by directly
80 using the six single components of the MT; however we follow the approach of Kikuchi and
81 Kanamori (1991) and parameterize the MT as a linear combination of six elementary MTs (M^m),
82 also known as Green's functions (GFs):

$$83 \quad M_{ij} = \sum_{m=1}^6 a_m M^m$$

$$84 \quad M^1 = \begin{bmatrix} 0 & 1 & 0 \\ 1 & 0 & 0 \\ 0 & 0 & 0 \end{bmatrix} \quad M^2 = \begin{bmatrix} 1 & 0 & 0 \\ 0 & -1 & 0 \\ 0 & 0 & 0 \end{bmatrix} \quad M^3 = \begin{bmatrix} 0 & 0 & 0 \\ 0 & 0 & 1 \\ 0 & 1 & 0 \end{bmatrix}$$

$$M^4 = \begin{bmatrix} 0 & 0 & 1 \\ 0 & 0 & 0 \\ 1 & 0 & 0 \end{bmatrix} \quad M^5 = \begin{bmatrix} -1 & 0 & 0 \\ 0 & 0 & 0 \\ 0 & 0 & 1 \end{bmatrix} \quad M^6 = \begin{bmatrix} 1 & 0 & 0 \\ 0 & 1 & 0 \\ 0 & 0 & 1 \end{bmatrix}$$

85 and from the a_m coefficients we can obtain the full moment tensor M:

$$86 \quad M_{ij} = \begin{bmatrix} a_2 - a_5 - a_6 & a_1 & a_4 \\ a_1 & -a_2 + a_6 & a_3 \\ a_4 & a_3 & a_5 + a_6 \end{bmatrix}$$

87 The advantage of using the elementary MT system over the single MT component is that
 88 the subgroups of this system have specific solutions that have direct physical meaning in their
 89 source mechanisms, such that we can parameterize the linear inversion into solving the generalized
 90 complete moment tensor that includes volumetric components using M^{1-6} or a purely deviatoric
 91 moment tensor using M^{1-5} (the five double-couple tensors) to estimate earthquake source
 92 parameters. 1D MT inversions follow the same approach as 3D except that GFs are defined
 93 following the Minson and Dreger (2008) formulation and calculated using frequency-wavenumber
 94 integration (e.g. Wang and Herrmann, 1980; Herrmann, 2012).

95 *Subsurface Velocity Structure*

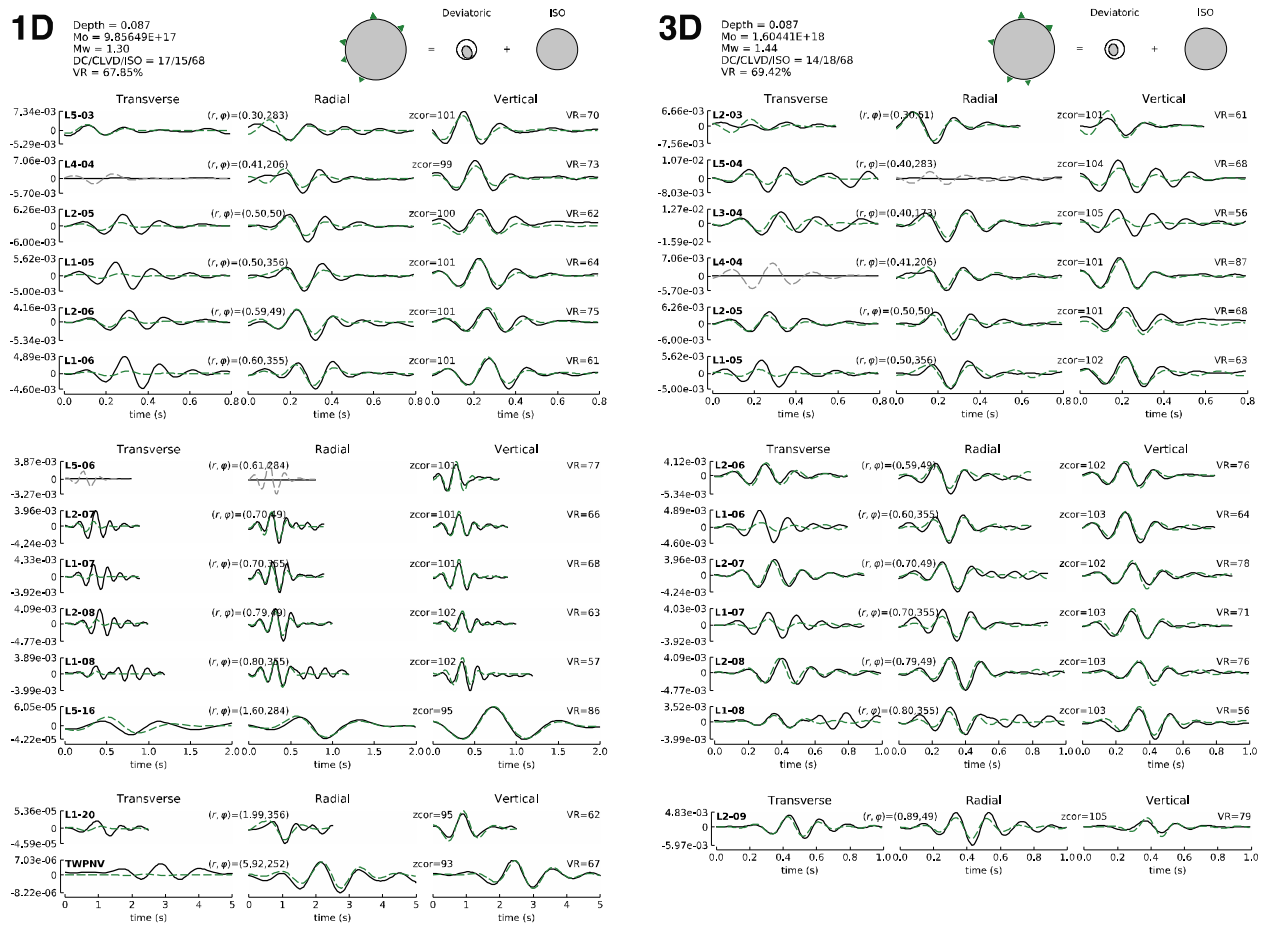
96 Subsurface velocity models are needed to simulate explosion wavefields and calculate the
 97 GFs for MT inversion. The reliability and robustness of the calculated source parameters are
 98 strongly dependent on our confidence in the detailed subsurface velocity structure.

99 The 1D model is based on granite properties and has a thin low velocity layer that
 100 represents the approximately 10 to 25 meter-thick highly fractured and weathered granite horizon
 101 observed in SPE geological and borehole data (Townsend et al., 2012). The 3D model, also known
 102 as the Geological Framework Model (GFM) is based on seismological (Pitarka et al., 2015),
 103 geological (Wagoner, 2014), and geophysical observations (Townsend et al., 2012). The top 200-
 104 m is a high-resolution 3D tomographic model developed using seismic interferometry (Matzel et
 105 al, 2016). Three techniques including ambient noise correlation (Hennino et al., 2001; Lobkis anf
 106 Weaver, 2001), shot interferometry, and coda wave interferometry (Campillo and Paul, 2003) were
 107 used to compute Green's function between seismometers and between the shots and seismometers.
 108 Each technique has its advantages over the other (e.g. frequency content, coverage, etc.) and
 109 collectively the three techniques give thousands of seismograms that cover the SPE site with the
 110 highest path densities along the five geophone lines. Similar to the 1D model a low velocity layer
 111 in the upper 30-m or so is observed in the 3D model but with more detailed structures laterally. At
 112 depth the 3D model transitions from tomography into a geological model that consists of
 113 Quaternary alluvium, Tertiary volcanic rocks, and Paleozoic sedimentary basement rocks with
 114 compressional wavespeeds from borehole data collected from the SPE site and various locations
 115 in Yucca Flat. We used the empirical relationships of Brocher (2005) to calculate shear
 116 wavespeeds and densities.

117 **Results**

118 The MT source model that fits most of the SPE Phase I series from both 1D and 3D
 119 inversions is a major ISO (explosion) source plus a minor deviatoric component (Figure 1). In
 120 general the deviatoric component can be decomposed into a combination of normal faulting and
 121 compensated-linear-vector-dipole (CLVD) with the major vector dipole in tension, and the
 122 strength of the deviatoric component is about 30% of the total seismic moment. The two instances
 123 that differ from this MT source model are SPE-5 and SPE-6 1D MT solutions. The variability in
 124 the deviatoric component from 1D MT is a result of fitting mostly radial and vertical components
 125 but not accurately predicting the transverse component. SPE data have substantial transverse
 126 motions sometimes with amplitudes comparable to the radial and vertical components. In the case
 127 where the 1D MT is fitting the transverse components (SPE-6) the solution becomes

130 predominantly CLVD, which is inconsistent with most other solutions in this study. The reduction
 131 of variability in the deviatoric component and improvement in predicting transverse motion from
 132 1D to 3D MT suggests the 3D Earth model is a better representation of the subsurface velocity
 133 structure, where uncertainties in source properties due to wave propagation effects are reduced.
 134 The 3D MTs also increase fits to waveforms along L3 and L4 where the arrays extend into
 135 alluvium deposits, and are not well-represented by the 1D granite model.
 136



137
 138 Figure 1. 1D and 3D moment tensor analysis of SPE-4P. The full moment tensor mechanism
 139 (lower hemisphere projection) are shown along with the deviatoric and isotropic (ISO)
 140 components. The diameter of the mechanism is related to its relative moment and the triangles
 141 around the circumference show the azimuthal coverage. Plotted below are data (solid black)
 142 compared with synthetics (dashed) predicted by the full mechanism filtered between 0.4 to 6 Hz.
 143 Gray dashed lines are predicted synthetics not included in the inversion. The station name, distance
 144 (r), azimuth (ϕ), time shifts (ZCOR, in number of points) and variance reduction (VR) are also
 145 shown for each station.
 146

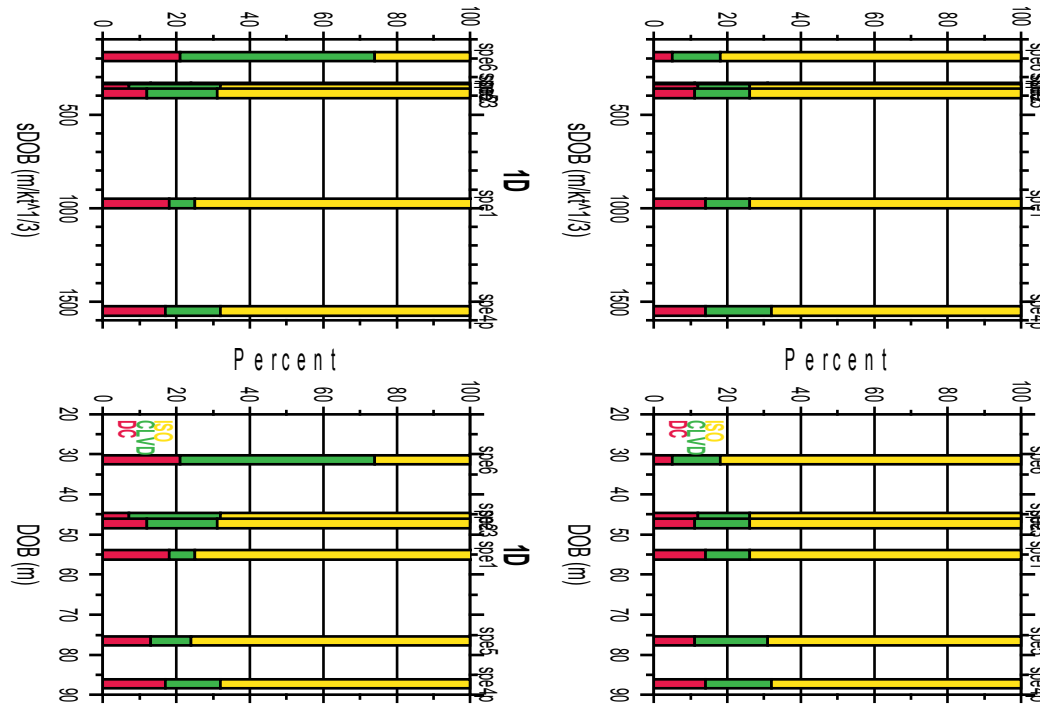
147 Table 1 and Figure 2 summarize the SPE Phase I source parameters from 1D and 3D MT
 148 analysis. The seismic moment predicted by 1D MT are consistently smaller compare to that of the
 149 3D due to minimal transverse energy predicted by the 1D mechanism. Generally, there is an
 150 improvement in the overall fits to the data in amplitude and phase (represented by the variance
 151 reduction, VR) from 1D to 3D, though it is not necessarily a one-to-one comparison since different
 152 stations were included in the 1D and 3D MT analysis. Instead of using a fixed set of stations for

153 all MT analysis we selected stations to maximize distance and azimuthal coverage for each analysis
 154 to obtain a well-constrained mechanism. The relative strength of the MT components is similar
 155 with respect to scaled depth of burial (sDOB) and depth of burial (DOB), and the anomalous
 156 solution of SPE-6 1D MT solution is more likely caused by errors in the velocity model and not
 157 necessarily the emplacement conditions. When we examine the individual MT elements we
 158 observe the Mzz component contributes to most of the variability seen in Figure 2.

159
 160 Table 1. SPE Phase I near source parameters and predicted seismic moment from full moment
 161 tensor analysis.

SHOT	YIELD (kg)	DEPTH (m)	sDOB (m/kt ^{1/3})	MODEL	Mo	Mw	VR (%)
SPE-1	90	55.1	976	1D	9.82231e17	1.29	51
				3D	1.59675e18	1.44	64
SPE-2	997	45.7	363	1D	1.51328e19	2.09	54
				3D	2.22615e19	2.20	58
SPE-3	905	47.2	387	1D	1.67337e19	2.12	57
				3D	2.45958e19	2.23	62
SPE-4P	89	87.2	1550	1D	9.85649e17	1.30	68
				3D	1.60441e18	1.44	69
SPE-5	5035	76.5	354	1D	6.00195e19	2.49	54
				3D	9.21861e19	2.61	53
SPE-6	2245	31.4	190	1D	2.12538e19	2.18	56
				3D	3.32300e19	2.31	55

162



163

164 Figure 2. 1D and 3D full moment tensor decomposition of SPE Phase I chemical experiments as
 165 a function of scaled depth of burial (sDOB) and depth of burial (DOB). The height of the vertical
 166 color bar relates to the relative strength of the isotropic (ISO, yellow), compensated-linear-
 167 vector-dipole (CLVD, green) and double-couple (DC, red) components.
 168

169 **Discussion**

170 *Forward Simulations from Hydrodynamic-to-Elastic Coupling*

171 A major improvement in ground motion simulation capabilities for explosion monitoring
 172 during SPE Phase I is the development of a wave propagation solver that can propagate explosion
 173 generated non-linear near field ground motions to the far-field. The advancement in ground motion
 174 simulation capabilities gives us the opportunity to assess MT inversion of a realistic volumetric
 175 source with near-field effects in a controlled setting, where we can evaluate the recovered source
 176 properties as a function of modeling parameters and can provide insights into source properties of
 177 SPE Phase I chemical experiments and other historical nuclear explosions.

178 The forward simulation combines the hydrodynamic modeling of the seismic source with
 179 elastic modeling of wave propagation. The calculation is done using a hybrid modeling approach
 180 with a one-way hydrodynamic-to-elastic coupling in three dimensions where near-field motions
 181 are calculated using GEODYN-L, a Lagrangian hydrodynamics code (Vorobiev, 2010; Vorobiev,
 182 2012), and then passed to WPP, as described previously.

183 The physics-based explosion source model used to simulate near-field, non-linear ground
 184 motions is a spherical explosion in a heavily jointed granite formation (Vorobiev et al., 2015;
 185 Vorobiev, 2017). The spatially varying joint and rock properties are inferred from experimental,
 186 geophysical and geological data collected as part of the SPE experiment (Townsend et al., 2012).
 187 The source region is characterized by a dominantly granitic outcrop and the resulting source model
 188 is developed through modeling near-field acceleration records from SPE Phase I, and multiple
 189 stochastic simulations were performed to capture the uncertainties resulted from the geological
 190 properties. Vorobiev et al. (2015) demonstrated that the movement along rock joints during
 191 explosion was the main mechanisms of shear wave generation in the near-field, however Pitarka
 192 et al. (2015) show that near-field source anisotropy and nonlinear effects combined with wave-
 193 scattering are needed to explain the observed far-field shear wave amplitudes and irregular
 194 radiation patterns.

195 SPE-4P, SPE-5 and SPE-6 physics-based source models were used in the coupled
 196 simulations. Similar to the MT analysis of actual SPE recordings, the preferred MT source model
 197 that fits the simulated data consists of a major ISO component and a minor deviatoric component
 198 (Figure 3, 3D/3D). The difference is that the deviatoric component is a CLVD mechanism with a
 199 vertically oriented vector dipole in tension and very little DC. In comparison to a pure ISO source,
 200 the additional CLVD improves the fits to the horizontals in terms of both phase and timing. There
 201 is a slight delay in phase arrival for a pure ISO model. Unlike S-wave generation in the near-field,
 202 most of the transverse energy seen in Figure 3 are due to 3D heterogeneities in the subsurface
 203 structure. If we propagate the same physics-based explosion volume source through a 1D Earth
 204 model less transverse energy is observed but the resulting MT source model is similar.
 205

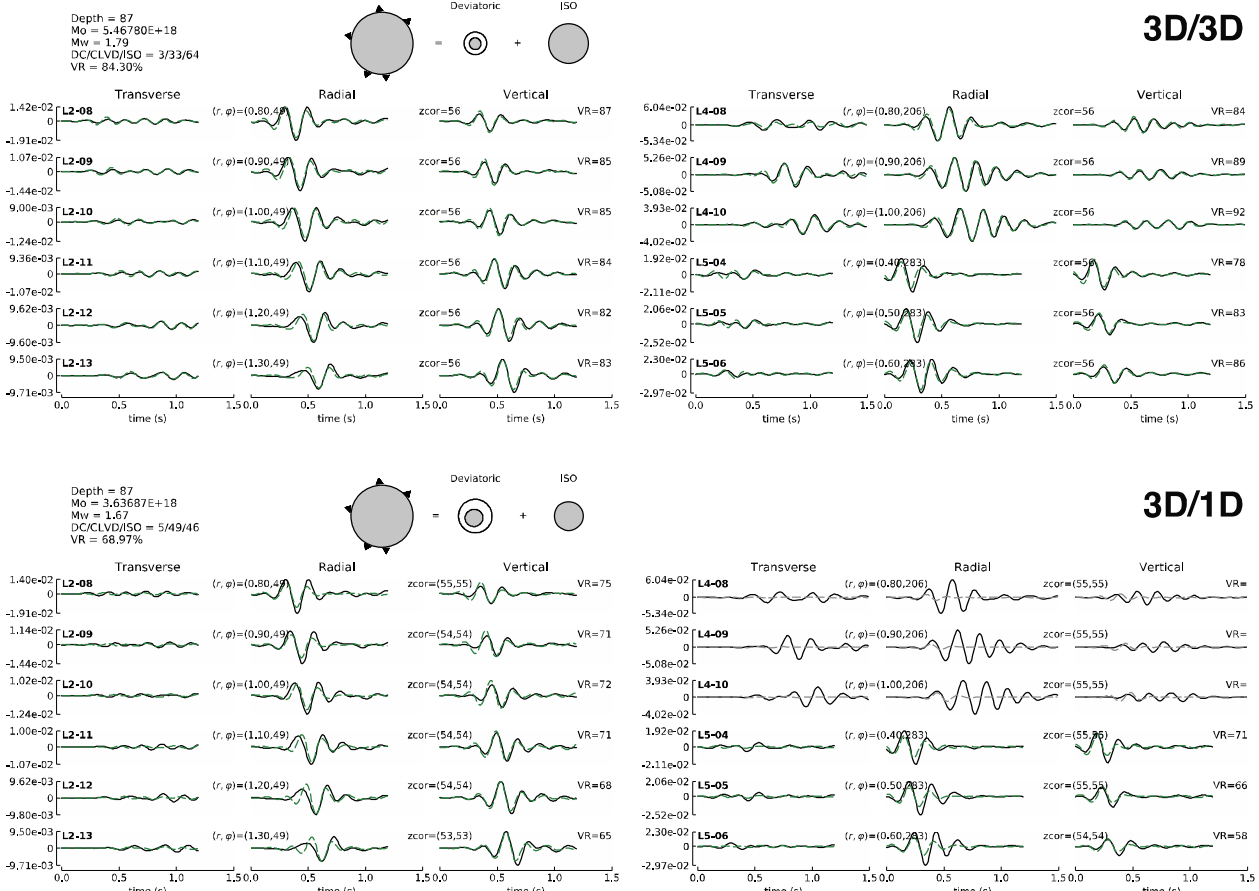


Figure 3. 3D and 1D moment tensor analysis of SPE-4P physics-based simulation. A subset of data (solid black) simulated from a physics-based explosion source model and propagated out to far-field distances using a 3D Earth model are plotted, as well as 3D (top, same model as data) and 1D (bottom) synthetics (dashed lines) predicted by the full mechanism. All data and synthetics are calculated with topography included and filtered between 2 to 6 Hz. Refer to Figure 1 for additional description.

When velocity model errors are introduced in the MT analysis (Figure 3, 3D/1D) the deviatoric to isotropic moment ratio tends to increase. There is also a change in the orientation of the major vector dipole where it is no longer vertically-oriented and the MT source model also fails to predict wave propagation along paths where the 3D model diverges from a simple 1D granite model, such as stations along L4. MT analysis of the physics-based, simulated wavefield reproduce the result from the analysis of actual SPE Phase I experiments. It implies scattering and phase conversion from 3D heterogeneities dominate the generation of far-field, low frequency (relative to near-field) transverse energy observed in data, and that the variability observed in the MT source model (Figure 1&2) are from inadequately accounting for wave propagation effects in the source inversion process.

Conclusions

A predominantly isotropic MT source model with a minor deviatoric component from 3D MT inversion best explains the observed far-field seismic wavefield produced by the SPE Phase I chemical experiments. Decomposition of the deviatoric component results in a combination of CLVD and normal mechanisms, and variability in the deviatoric component and the relative

strengths of the MT elements are largely the result of inadequately accounting for 3D wave propagation effects in the source inversion process. S-wave generation in the far-field is dominated by scattering and phase conversion from 3D heterogeneities in the subsurface and not the MT source. These observations are supported by modeling of physics-based seismic wavefield simulations from hydrodynamic-to-elastic coupling in which the preferred MT source model for a realistic volumetric explosion with nonlinear source properties is predominately isotropic with a vertically-oriented CLVD in tension.

236

Acknowledgement

This work was sponsored by NNSA DNN R&D under award number DE-AC52-06NA25946. Lawrence Livermore National Laboratory is operated by Lawrence Livermore National Security, LLC, for the U.S. Department of Energy, National Nuclear Security Administration under Contract DE-AC52-07NA27344. LLNL-TR-767905. LLNL-TR-767905

242

References

Aki, K. and P. G. Richards (2002). Quantitative Seismology, 2nd edition. University Science Books.

Campillo M and A. Paul (2003). Long-range correlations in the diffuse seismic coda, *Science* 299(5606), 547-549.

Denny, M. D. (Editor) (1994). Proc. Of the Symposium on the Non-Proliferation Experiment (NPE): Results and Implications for the Test Ban Treaties, 19-21 April 1994, Rockville, Maryland, CONF 9404100, Lawrence Livermore National Laboratory.

Guilhem, A., L. Hutchings, D. S. Dreger and L. R. Johnson (2014). Moment tensor inversions of M~3 earthquakes in the Geysers geothermal fields, California, *J. Geophys. Res.* 119(3), doi:10.1002/2013JB010271

Hennino R., N. Trégourès, N. M. Shapiro, L. Margerin, M. Campillo, B. A. van Tiggelen, and R. L. Weaver (2001). Observations of equipartition of seismic waves, *Phys. Rev. Lett.* 86, 3447.

Herrmann, R. B. (2013). Computer programs in seismology: An evolving tool for instruction and research, *Seism. Res. Lettr.* 84, 1081-1088, doi:10.1785/0220110096

Johnson, L.R., and C.G. Sammis, (2001), Effects of rock damage on seismic waves generated by explosions, *Pageoph* 158, 1869–1908.

Kikuchi M. and H. Kanamori (1991). Inversion of complex body waves-III, *Bull. Seismol. Soc. Am.* 81(6), 2335-2350.

Lobkis, O.I. and R. L .Weaver (2001). On the Emergence of the Green's Function in the Correlations of Diffuse Field. *The Journal of the Acoustical Society of America*, 110, 3011-3017. <https://doi.org/10.1121/1.1417528>

Matzel E. M., A. Pitarka and R. J. Mellors (2016). Seismic imaging of the source physics experiment using seismic interferometry, *International Seismix Symposium*.

McNamara, D. E., H. M. Benz, R. B. Herrmann, E. A. Bergman, P. Earle, A. Holland, R. Baldwin, and A. Gassner (2015). Earthquake hypocenters and focal mechanisms in central Oklahoma reveal a complex system of reactivated subsurface strike-slip faulting, *Geophys. Res. Lett.* 42(8), 2742–2749, doi:10.1002/2014GL062730.

Minson, S. E. and D. S. Dreger (2008). Stable inversions for complete moment tensors, *Geophys. J. Int.* 174, 585-592.

Minson, S. E., D. S. Dreger, R. Bürgmann, H. Kanamori, and K. M. Larson (2007), Seismically and geodetically determined nondouble-couple source mechanisms from the 2000

274

275 Miyakejima volcanic earthquake swarm, *J. Geophys. Res.*, 112, B10308,
276 doi:[10.1029/2006JB004847](https://doi.org/10.1029/2006JB004847).

277 Nilsson, S., N.A. Petersson, B. Sjogreen and H.-O. Kreiss (2007). Stable difference
278 approximations for the elastic wave equation in second order formulation, *SIAM J. Numer.*
279 *Anal.* v. 45, pp 1902-1936.

280 Patton, H. (2012). Have the effects of material damage been detected in Rg waveforms recorded
281 on SPE-1 and -2? Los Alamos National Laboratory, LA-UR-12-22068.

282 Patton, H. J., J. L. Bonner, and I. N. Gupta (2005). Rg excitation by underground explosions:
283 insights from source modelling the 1997 Kazakhstan depth-of-burial experiment, *Geophys.*
284 *J. Int.* 163, 1006-1024.

285 Pitarka A., R.J. Mellors, W.R. Walter, S. Ezzedine, O. Y. Vorobiev, T. Antoun, J. L. Wagoner, E.
286 M. Matzel, S. R. Ford, A.J. Rodgers, L. Glenn and M. Pasmanos (2015). Analysis of ground
287 motion from an underground chemical explosion. *Bull. Seismol. Soc. Am.* 105 (5): 2390–
288 2410. doi: <https://doi.org/10.1785/0120150066>

289 Snelson, C. M., R. E. Abbott, S. T. Broome, R. J. Mellors, H. J. Patton, A. J. Sussman, M. J.
290 Townsend and W. R. Walter (2013), Chemical Explosion Experiments to Improve Nuclear
291 Test Monitoring, *Eos Trans. AGU*, 94(27), 237.

292 Shuler, A., M. Nettles and G. Ekström (2013), Global observation of vertical-CLVD earthquakes
293 at active volcanoes, *J. Geophys. Res. Solid Earth*, 118, 138–164,
294 doi:[10.1029/2012JB009721](https://doi.org/10.1029/2012JB009721).

295 Townsend, M., L. B. Prothro and C. Obi (2012). Geology of the Source Physics Experiment Site,
296 Climax Stock, Nevada National Security Site. doi:[10.2172/1036766](https://doi.org/10.2172/1036766).

297 Wagoner, J. L. (2014). Working toward a site-specific geomodel, Nevada National Security Site,
298 RMR2014—Review of Monitoring Research for Ground-Based Nuclear Explosion
299 Monitoring Technologies, Albuquerque, New Mexico, 18 June 2014.

300 Wallace, T., D. Helmberger and G. Engen (1985). Evidence for tectonic release from underground
301 nuclear explosions in long period S waves, *Bull. Seism. Soc. Am.*, 75: 157–174.

302 Wang, C.Y., and R.B. Herrmann (1980). A numerical study of P-, SV-, and SH-wave generation
303 in a plane layered medium, *Bull. Seismol. Soc. Am.* 70(4), 1015-1036.

304 Xu, H., A. J. Rodgers, I. N. Lomov, and O. Y. Vorobiev (2014). Seismic source characteristics
305 from simulations of nuclear and chemical explosions in Granite, *Pure Appl. Geophys.* 171,
306 507–521,

307 Vorobiev, O. Y. (2010). Discrete and continuum methods for numerical simulations of non-linear
308 wave propagation in discontinuous media, *Int. J. Numer. Meth. Eng.* 83, 482–507.

309 Vorobiev, O. Y. (2012). Simple common plane contact algorithm, *Int. J. Numer. Meth. Eng.* 90,
310 243–268.

311 Vorobiev, O. Y. (2017). Two sources of nonisotropic radiation from underground explosions in
312 granite. *Journal of Geophysical Research: Solid Earth*, 122, 9109–9117.
313 <https://doi.org/10.1002/2017JB014718>

314 Vorobiev, O. Y., S. Ezzedine, T. Antoun and L. Glenn (2015). On the generation of tangential
315 ground motion by underground explosions in jointed rocks. *Geophys. J. Int.* 200(3), 1651–
316 1661.

317

318